Heat and Mass Transfer (2019) 55:1195–1205
https://doi.org/10.1007/s00231-018-2496-y

ORIGINAL

Experimental and numerical investigation of heat transfer characteristics in an internally circulating fluidized bed

Lijun Wang[1] · Weiwei Yuan[1] · Shuping Duan[1] · Jiajun Sun[1] · Lingfeng Xu[1]

Received: 15 July 2018 / Accepted: 29 September 2018 / Published online: 17 October 2018

Abstract

The heat transfer performance of a tube heat exchanger has great significance for the metal smelting, catalytic cracking and combustion performance in the fluidized bed reactor. In this paper, a three dimensional Eulerian–Eulerian simulation for the vertical heater tube to bed heat transfer within a baffle type internal circulating fluidized bed (ICFB) was conducted numerically and the results were compared to experimental ones. Gidaspow's drag correlation was adopted to describe the interaction between the gas and solid phases in the ICFB. Temperature and heat transfer coefficient were numerically analyzed under different operating conditions as same as the experimental setup. The effects on the heat transfer characteristic of input heat flux, air inlet velocity, and initial solid packing height were investigated as the average temperature was compared with the experimental data in the literature. The simulation results showed that along the height of the bed, the velocity of the solid particles increases, lateral movement of the particles from the low-speed area to the high-speed area can be observed at the bottom of the acceleration area. The convective heat transfer coefficient of solid particles is the main component of heat transfer in the dense phase zone, with the increase of the initial solid packing height, the average convection heat transfer coefficient between the fluid and the heated surface is shown an upward trend. By comparing the experimental datas, it can be concluded that the numerical simulation of the flow and heat transfer process of the inner circulating fluidized bed by the Eulerian-Eulerian method is in good agreement with the experimental results.

Nomenclature

C_D	Drag coefficient
d_s	Diameter of particles
e	Restitution coefficient
h	Heat transfer coefficient
H	Height of bed
k	Thermal conductivity
K	Interphase momentum exchange coefficient
p	Pressure
q	Heat flux
Γ,ω,A,B	Factors of effective thermal conductivity
Ψ	Specific enthalpy
μ	Viscosity
ε	Volume fraction

Subscripts/superscripts

avg	Averaged
eff	Effective
exp	Experimental
f	Fluid
g	Gas phase
i	The measuring point of variables
mf	Minimum fluidization
num	Numerical
s	Solid phase
w	Heater wall

✉ Lijun Wang
wanglijun@sau.edu.cn

[1] College of Energy and Environment, Shenyang Aerospace University, Shenyang, China

1 Introduction

Compared to the circulating fluidized bed, the internal circulating fluidized bed (ICFB) has many advantages, such as compact structure, relatively low heat loss [1] from the reactor and flexible operation due to its structure. Therefore, ICFB has been widely used in various processes, such as coal combustion and co-combustion [2, 3], coal gasification [4], incineration of solid waste, and continuous adsorption and desulfurization [5]. It is indispensable to study the heat transfer characteristics in the ICFB aiming to obtain high combustion efficiency, which requires the temperature in the bed should be controlled in a certain range. Due to the high temperature of the combustion

chamber, it is very difficult to make specific measurements for the detailed study of gas-solid flow by using industrial-scale ICFB. In past decades, with the developments in the computational power and numerical algorithms, the distribution of temperature, pressure, and velocity in the fluidized bed can be obtained through the computational fluid dynamics(CFD) [6].There are a lot of numerical studies on the flow characteristics of granular [7–9], whereas, the CFD simulation including heat transfer research in ICFB can be rarely found. Therefore, it is essential to propose a suitable calculation model for predicting the heat transfer characteristics in ICFB.

Heat transfer between the bed particles and tube surfaces in ICFB is influenced by many factors, such as the size and physical properties of the bed particles, size of the tube and the placement of tube and so on. Besides, some operating parameters, such as temperature, pressure and fluidization speed, also affect the heat transfer process. Two-Fluid model (TFM) was adopted by Lu [10] to model the heat transfer and solid volume fraction distribution characteristics in a supercritical water (SCW) fluidized bed with the immersed tube. Moreover, the Gidaspow drag model and Gunn heat transfer correlation are used to describe the interaction and heat transfer between different phases, respectively. Wang et al. [11] confirmed that the gidaspow drag model is more suitable for this study than other drag models. Leinaal et al. [12] numerically studied the fluidization characteristics and hydrodynamics with an irregular particle in dense gas-solid fluidized bed reactors using the TFM. The combined approach of discrete element method (DEM) and computational fluid dynamics (CFD) is extended to study the flow and thermal behavior in packed and fluidized beds of ellipsoids by. Jieqing Gan et al. [13]. N.H. Dong et al. [14] using TFM numerically studies the effect of tube shape on the hydrodynamics and tube-to-bed heat transfer in fluidized beds, which reveals that the heat transfer coefficient varies sensitively with the distribution of the solid phase. The studies by Olsson and Almstedt [15] showed that the frequency of exchange of particles at the surface and the particle concentration near the surface play an important role in the estimation of the heat transfer coefficient.

Many experimental and numerical studies revealed the flow and mixing characteristics in the fluidized bed reactor. However, the research on heat transfer characteristics in ICFB lacks in the literature. In this paper, the Eulerian-Eulerian (E-E) approach was employed to simulate the convective heat transfer coefficient between the vertical heater tube and the bed mixture under different operating conditions within a baffle type internal circulating fluidized bed. Moreover, Gidaspow [16] drag model correlation is adopted to describe the interaction of inter-phases and the comparison of results from experimental and numerical approaches is carried out to prove that the numerical process is feasible. Meanwhile, it provides theory evidence in heat transfer process design, control and/or optimization for the effective industrial applications of ICFB.

2 Experiment setup

2.1 Equipment and measurements

The experimental setup of ICFB used in this paper mainly aims to measure the temperature of the fluid and the columnar heater wall in ICFB as shown in Fig. 1. In order to improve the diffusion of particles in the fluidized bed and to enhance the fluidization of gas and solid phase, the uniform air was distributed to the lateral side of the fluidized zone under the condition of non-uniform air distribution at the bottom of the fluidized bed. The main system is composed of an organic glass fluidized bed, blast components, pressure measuring modules, resistance-type heater, thermocouple components, and control device. According to the different position and air inlet velocity, the distributor of inlet-air is named as high-speed air intake U_H, low-speed air intake U_L, and facilitated air intake U_F, which are used to study the combined effect of different position and inlet velocity on the temperature characteristics of the bed. The geometric dimensions of the cold experimental model of ICFB are shown in Fig. 2. Quartz sand particles with the equivalent diameter range of 0.100–0.500 mm were used as the bed material of a fluidized bed. In the process of experiment, both the temperature and the velocity of inlet air are regulated by the electronic regulator. The temperature is measured by the HT9815 thermocouple, the digital temperature measurement range is from −200 °C to 1372 °C, the test resolution is 0.1 °C, the measuring error is 1% and the location of measuring point is shown as Fig. 2b.

2.2 Solid mass flux across the opening orifice

The solid mass flux of particles(W) across the opening orifice in the circulating fluidized bed has a significant

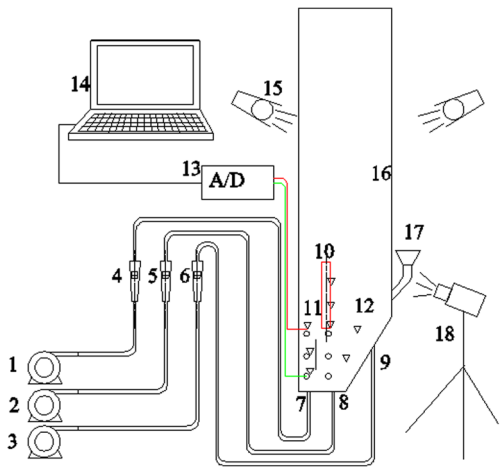

Fig. 1 The schematic diagram of experimental system: (1,2,3) air blower;(4,5,6) rotary flow meter;(7,8,9) air distributor; (10) resistance type heater; (11)pressure sensor (circle); (12)temperature sensor(triangle); (13) A/D convert; (14) computer; (15) floodlight; (16) ICFB; (17) worm feeder; (18)high speed digital camera

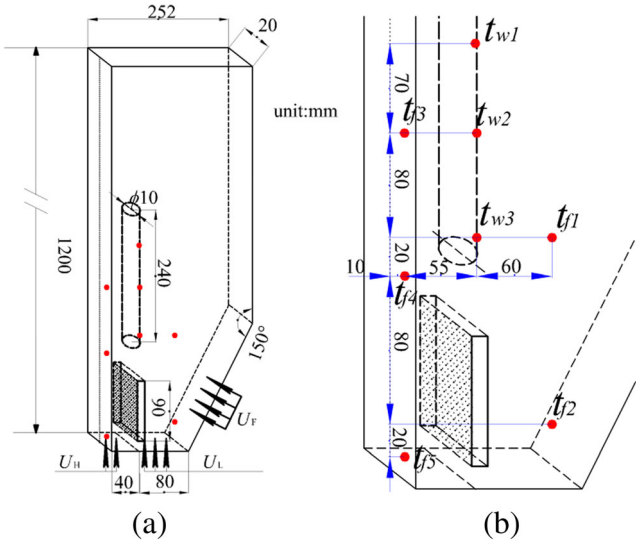

Fig. 2 Geometric dimension of the Plexiglas cold model and aeration process(a) and locations of thermocouples (b)

influence on the fluid flow, temperature control, heat and mass transfer in the bed. Kuramoto et al. [17] obtained a formula for the solid mass flux of particles by summarizing a large number of experimental data, which can be expressed as below:

$$W = C_{s0}\varepsilon_u^{2.35}(2\rho_d \Delta P_0)^{1/2} \quad (1)$$

where $C_{so} \leq 0.1$ is the discharge coefficient, ε_u is the voidage of up-flowing bed, ρ_d is the density of the down-flowing bed, and ΔP_0 is the pressure difference, respectively.

2.3 Determination of inlet gas velocity

ICFB experimental bench adopts three positions of high, low and facilitate for air distribution. The initial fluidization velocity corresponding to the particle diameter ds = 0.500 mm is 0.205 m/s. The air inlet velocity is defined as the ratio between the actual inlet volume flow rate (m3/s) and cross-sectional area (m2) at the calculated cross-section. The air inlet velocities at different positions applied in the experiment are calculated in Table 1.

3 Numerical model and simulation setting

3.1 Eulerian-Eulerian model

The two-fluid model (TFM) is widely used to simulate the hydrodynamics and heat transfer in the dense phase fluidized bed. Both the gas phase and the solid phase are considered as continuous phases and have their own independent volume fractions within the grid of the control unit in the Eulerian model, which was based on the kinetic theory of granular flow [18] that the pressure and viscosity of the solid phase depend on the magnitude of particle velocity fluctuations characterized by the granular temperature. The Gidaspow drag function (combined with the Wen-Yu [19] and Ergun [20] models) is used in this paper, together with the governing equations and constitutive equations of Eulerian approach listed in Table 2. Besides, the radiative heat transfer component was neglected since the operating temperature in the fluidized bed is about 20–300 °C (less than 600 °C) [21] during the experiment. Therefore, the convective heat transfer between the fluid mixture and the heater wall was mainly considered in this paper. All of the equations as described in Tables 2 and 3 were solved by using commercial software Ansys Fluent.

3.2 Simulation conditions

The Eulerian-Eulerian model was implemented using the commercially available Computation Fluid Dynamics software FLUENT17.0 (ANSYS, Inc., USA). No-slip and adiabatic boundary conditions were applied at the wall for both sand and air. Constant heat flux conditions were adopted on the surface of the heater wall. The air inlet located at the bottom of the bed was designated as a velocity inlet, and the boundary condition at the top of ICFB was specified as pressure outlet. The phase coupled SIMPLE algorithm was used for pressure and velocity coupling. In order to improve accuracy, the second-order upwind scheme was adopted to discretize the governing eqs. A time step of 0.001 s was applied for the transient model, and within each time step, a residual of less than 10–3 for the continuity equation was imposed as the stopping criterion. A total time of 10 s was simulated to ensure that the flow and heat transfer inside the ICFB reached steady states. Other physical properties of the

Table 1 The velocity of the air inlet in the simulations (U_F = 0.68 m/s)

Initial solid packing height H(cm)	20	Heat flux q(W/m^2)		46,419
	Superficial gas velocity(m/s)			
U_H	1.74	1.74	2.57	2.57
U_L	0.87	0.69	0.87	0.69
Difference of air inlet Velocity U_H - U_L(m/s)	0.87	1.05	1.70	1.88
Total volume flow of air inlet Q(m^3/h)	10.0	9.0	12.4	11.4

Table 2 Governing equations and drag function

Continuity equation

$$\frac{\partial}{\partial t}\left(\varepsilon_g\rho_g\right)+\nabla\cdot\left(\varepsilon_g\rho_g\vec{v}_g\right)=0 \quad (2)$$

$$\frac{\partial}{\partial t}\left(\varepsilon_s\rho_s\right)+\nabla\cdot\left(\varepsilon_s\rho_s\vec{v}_s\right)=0 \quad (3)$$

Volume fraction

$$\varepsilon_g+\varepsilon_s=1 \quad (4)$$

The momentum equations for solid and gas phases

$$\frac{\partial}{\partial t}\left(\varepsilon_g\rho_g\vec{v}_g\right)+\nabla\cdot\left(\varepsilon_g\rho_g\vec{v}_g\vec{v}_g\right)=-\varepsilon_g\nabla p+\nabla\cdot\bar{\bar{\tau}}+\varepsilon_g\rho_g\vec{g}+K_{sg}\left(\vec{v}_s-\vec{v}_g\right) \quad (5)$$

$$\frac{\partial}{\partial t}\left(\varepsilon_s\rho_s\vec{v}_s\right)+\nabla\cdot\left(\varepsilon_s\rho_s\vec{v}_s\vec{v}_s\right)=-\varepsilon_s\nabla p+\nabla p_s+\nabla\cdot\bar{\bar{\tau}}_s+\varepsilon_s\rho_s\vec{g}+K_{gs}\left(\vec{v}_g-\vec{v}_s\right) \quad (6)$$

Conservation of energy

$$\frac{\partial\left(\varepsilon_g\rho_g\psi_g\right)}{\partial t}+\nabla\cdot\left(\varepsilon_g\rho_g\psi_g\vec{v}_g\right)=-\varepsilon_g\frac{\partial p_g}{\partial t}+\bar{\bar{\tau}}_g:\nabla\vec{v}_g-\nabla\cdot q_g+S_g+h_{gs}\left(T_g-T_s\right) \quad (7)$$

$$\frac{\partial\left(\varepsilon_s\rho_s\psi_s\right)}{\partial t}+\nabla\cdot\left(\varepsilon_s\rho_s\psi_s\vec{v}_s\right)=-\varepsilon_s\frac{\partial p_s}{\partial t}+\bar{\bar{\tau}}_s:\nabla\vec{v}_g-\nabla\cdot q_s+S_s+h_{sg}\left(T_s-T_g\right) \quad (8)$$

Gidaspow drag function

$$K_{sg}=\frac{3}{4}C_D\frac{\varepsilon_s\varepsilon_g\rho_g\left|\vec{v}_s-\vec{v}_g\right|}{d_s}\varepsilon_g^{-2.65},\ \varepsilon_s \text{ for } \varepsilon_g>0.8 \quad (9)$$

$$C_D=\frac{24}{\varepsilon_g\mathrm{Re}_s}\left[1+0.15\left(\varepsilon_g\mathrm{Re}_s\right)^{0.687}\right] \quad (10)$$

$$K_{sg}=150\frac{\varepsilon_s\left(1-\varepsilon_g\right)\mu_g}{\varepsilon_g d_s^2}+1.75\frac{\rho_g\varepsilon_s\left|\vec{v}_s-\vec{v}_g\right|}{d_s} \quad \text{for } \varepsilon_g\leq 0.8 \quad (11)$$

$$\mathrm{Re}_s=\frac{\rho_g d_s\left|\vec{v}_s-\vec{v}_g\right|}{\mu_g} \quad (12)$$

bed material and the specific parameter settings in the numerical simulations were the same as those used in the experiments, as seen in Table 4.

4 Numerical validation

Since the numerical simulation of the internal circulating fluidized bed temperature field is based on the coupling between heat transfer and flow field, it is very important to ensure the numerical simulation results of the flow field consistent with the actual situation. Therefore, before performing CFD simulation, we need to compare the particle flow trajectory and concentration distribution obtained from the simulation and the flow field image obtained from the experimentation. The selected operating conditions are given as $U_H = 2.57$ m/s, $U_L = 0.69$ m/s, $U_F = 0.68$ m/s, Q = 10.0 m3/h, H = 20 cm, q = 46,419 W/m2. Figure 3 shows the comparison chart between the internal circulating fluidized bed experiment and the numerical simulation flow field. It can be seen from the simulated flow field diagram that the violent turbulent motion of the quartz sand particles in the fluidized bed. Comparing the flow field structures of the two types of graphs, it can be observed that the concentration distribution of the transient particles obtained at the same moment in the experiment is not fully consistent with the results obtained from the simulation. Only some of the flow field characteristics are similar. This is due to the fact that the turbulent motion is physically characterized by infinitely large scales and mathematically strong nonlinearities, and making the turbulent motion a certain randomness. Figure 4 shows the changes in the temperature of the fluidized bed heating wall and the average particle cluster temperature with time at different simulation times. Under the same working conditions as Fig. 3, it can be found that the temperature of the heater wall surface and fluid particle cluster obtained by the simulation reaches a steady state when the simulation time reaches to 10 s. Referring to the average temperatures obtained by experiments such as Shedid and Hassan [17], the relative error is controlled with

Table 3 Heat transfer coefficient (HTC)

Numerical method for calculating HTC

$$h_{num}=\frac{q}{t_{w,num}-t_{f,num}}=\frac{\varepsilon_s k_{s,eff}\left|\frac{\partial t_s}{\partial n}\right|+\varepsilon_g k_{g,eff}\left|\frac{\partial t_g}{\partial n}\right|}{t_{w,num}-t_{f,num}} \quad (13)$$

$$k_{g,eff}=\left(\frac{1-\sqrt{\varepsilon_s}}{\varepsilon_g}\right)k_g \quad (14)$$

$$k_{s,eff}=\frac{1}{\sqrt{\varepsilon_s}}k_g\left[\omega A+(1-\omega)\,\Gamma\right] \quad (15)$$

$$\Gamma=\frac{2}{1-B/A}\left[\frac{A-1}{(1-B/A)^2}\frac{B}{A}\ln\left(\frac{A}{B}\right)-\frac{B-1}{1-B/A}-\frac{B+1}{2}\right] \quad (16)$$

$$A=k_s/k_g,\ B=1.25(\varepsilon_s/\varepsilon_g)^{10/9},\ \omega=7.26e^{-3} \quad (17)$$

$$h_{\exp}=\frac{q}{t_{w,\exp}-t_{f,\exp}} \quad (18)$$

$$t_{w,num}=\frac{1}{3}\sum_{i=1}^{3}t_{w\,i} \quad (19)$$

$$t_{w,\exp}=\frac{1}{3}\sum_{i=1}^{3}t_{w\,i} \quad (20)$$

$$t_{f,num}=\frac{1}{5}\sum_{i=1}^{5}t_{f\,i} \quad (21)$$

$$t_{f,\exp}=\frac{1}{5}\sum_{i=1}^{5}t_{f\,i} \quad (22)$$

Table 4 Physical and numerical parameters

Parameter	Value
Air density, ρ_g (Kg/m^3)	1.225
Particle density, ρ_s (Kg/m^3)	2650
Gas inlet volumetric flow rate, Q (m^3/h)	9.0、10.0、11.4、12.4
Particle diameter, d_s (mm)	0.1–0.5
Minimum fluidization velocity for $d_s = 0.5$ mm, U_{mf}(m/s)	0.210
Heat flux, q (W/m^2)	19,894、37,135、46,419、50,398
Initial solid packing heights, H (cm)	20
Restitution coefficient e	0.9
Initial packing rate β	0.55
Gas phase thermal conductivity, k_g (W/(mK))	0.0252
Solid phase thermal conductivity, k_s (W/(mK))	0.9
Gas phase specific heat at constant pressure, $C_{p,g}$(J/(kgK))	1005
Solid phase specific heat at constant pressure, $C_{p,s}$(J/(kgK))	865
Air viscosity kg/ms μ_g(kg/ms)	1.79e^{-5}
Inlet	Velocity inlet
Outlet	Pressure outlet
Wall	Adiabatic, no-slip for fluid
Heater wall	Constant heat flux(q), no-slip for fluid

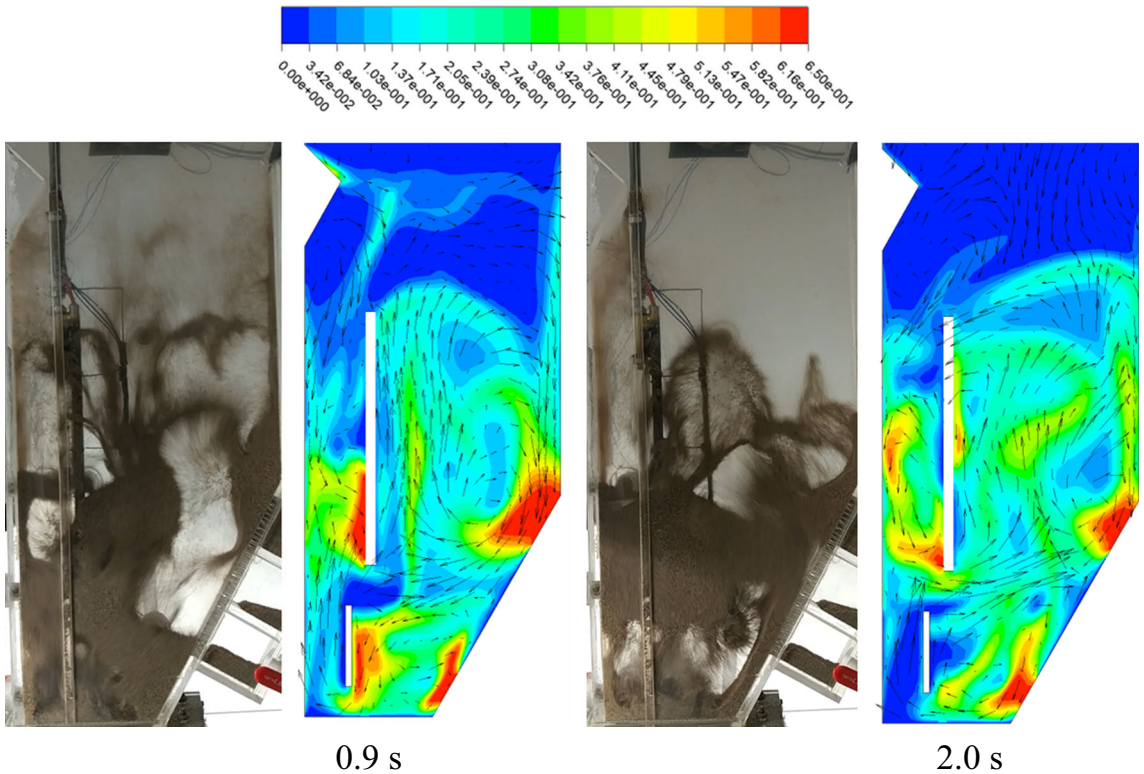

Fig. 3 The comparison of particle motion images between simulations and experiments at different numerical time (U_H = 2.57 m/s, U_L = 0.69 m/s, U_F = 0.68 m/s, Q = 10.0 m^3/h, H = 20 cm, q = 46,419 W/m^2)

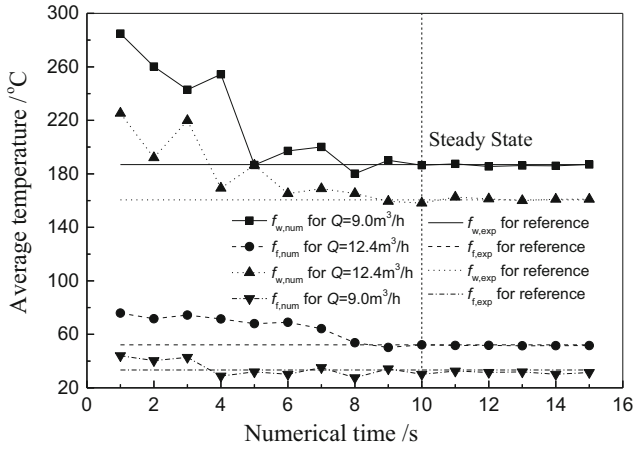

Fig. 4 Variation of wall and bulk average temperature at different numerical time. (U_H = 2.57 m/s, U_L = 0.69 m/s, U_F = 0.68 m/s, Q = 10.0 m^3/h, H = 20 cm, q = 46,419 W/m^2)

6.4%, which verifies the feasibility of the two-fluid heat transfer model.

5 Results and discussion

5.1 Flow characteristic

Figure 5 shows the numerical simulation results of particle phase volume fraction and velocity vector graphs at different times in the internal circulating fluidized bed based on experimentally validated numerical simulation methods. During the simulation time 0.1–0.5 s, it can be observed that a moment of the high-speed inlet air enters the bottom of the bed from the distribution plate to form a large gas collection, and the solid-phase particles above the collection area acquire a certain rising speed. However, after 0.1 s, the particle velocity almost dropped to zero (the length of the vector corresponding to the 0.2 s chart was almost zero), and the concentration of particles decreased and the voidage increased in the center area above the gas collection in the period of 0.3–0.5 s. The particles mainly move upwards, and the local airflow velocity increases; while near the wall surface, the particle concentration gradually increases, and the particles mix back downwards to form an internal circulation flow structure. From the time of 0.8–2.0 s of the numerical simulation results, it can be observed that a rapid mix fluidization process from high-speed gas flow into the gas-solid phase in the hearth has formed relatively stable turbulent fluidization. Compared to the bubble formation and crushing process in a bubbling fluidized bed, it is difficult to observe the basic characteristics of the fast bubble and slow bubble structure in the bubbling bed flow in the bottom of the internal circulating fluidized bed. According to the morphological characteristics of the flow field, the fluidization type of the dense phase area in the lower part of the inner circulating fluidized bed belongs to the turbulent bed.

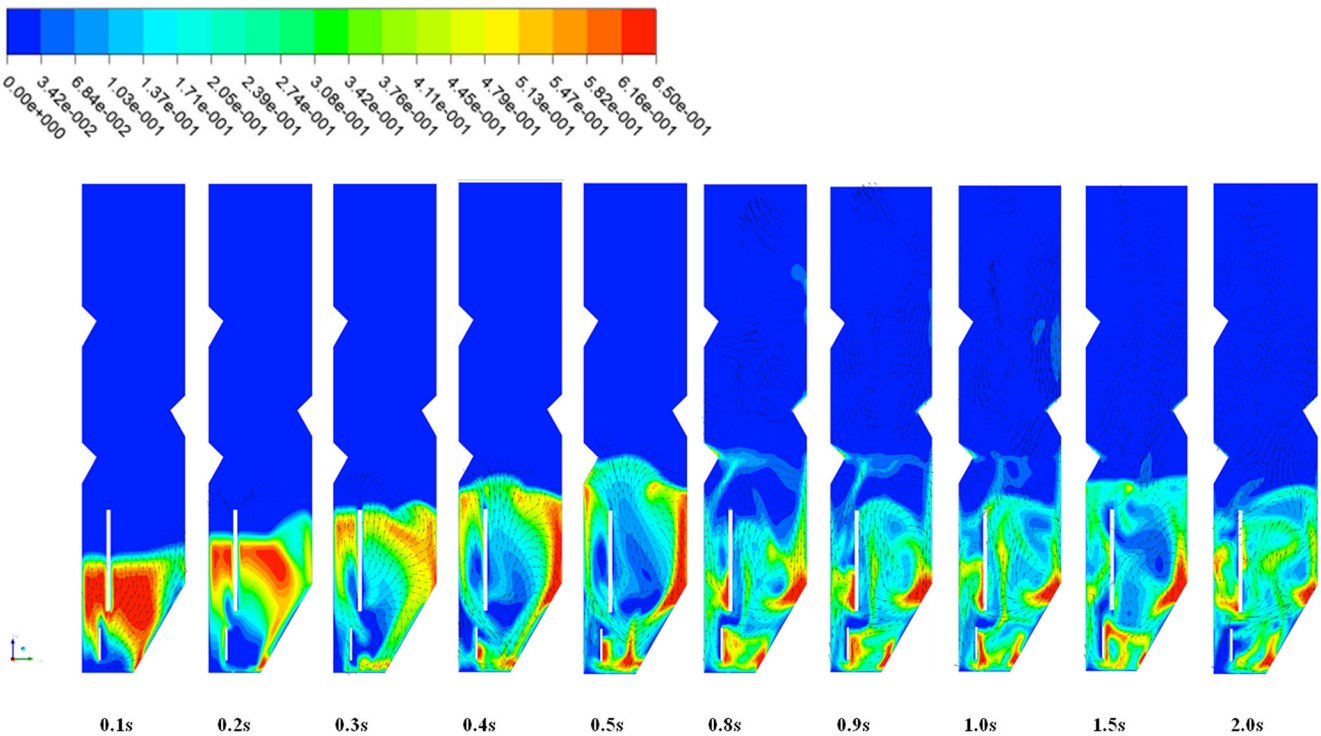

Fig. 5 Contour plot of transient distribution of solid volume fraction and velocity vector at different numerical time (U_H = 2.57 m/s, U_L = 0.69 m/s, U_F = 0.68 m/s, Q = 10.0 m^3/h, H = 20 cm, q = 46,419 W/m^2)

5.2 Effect on heat transfer of solid volume fraction around heater surface

In the dense-phase region of the lower part of the circulating fluidized bed, the mixing between the gas-solid phases is violent, and the flow state generally belongs to the turbulent flow state. For the further study of the convective heat transfer details of the heater accessories, in this paper, the convective heat transfer coefficients of different heating tube positions at six-time points within 0.1–0.6 s were compared and analyzed. Figure 6 shows the distribution of solid particle volume fraction near the heating surface at different times and the convective heat transfer coefficient of the right side of the heater. The selected operating conditions were $U_H = 2.57$ m/s, $U_L = 0.69$ m/s, $U_F = 0.68$ m/s, Q = 10.0 m3/h, H = 20 cm, q = 46,419 W/m2. From Eq. 12, it can be found that the heat transfer between the heater surface and the fluid includes the convective heat transfer of both the gas phase and the solid phase. From the observations of Fig. 0.1 s and 0.2 s, it can be found that the local convection heat transfer coefficient of the heater with high voidage (high gas volume fraction) is very low because of the low effective thermal conductivity of the gas phase. Overview of the whole picture (0.1–0.6 s), it is readily found that

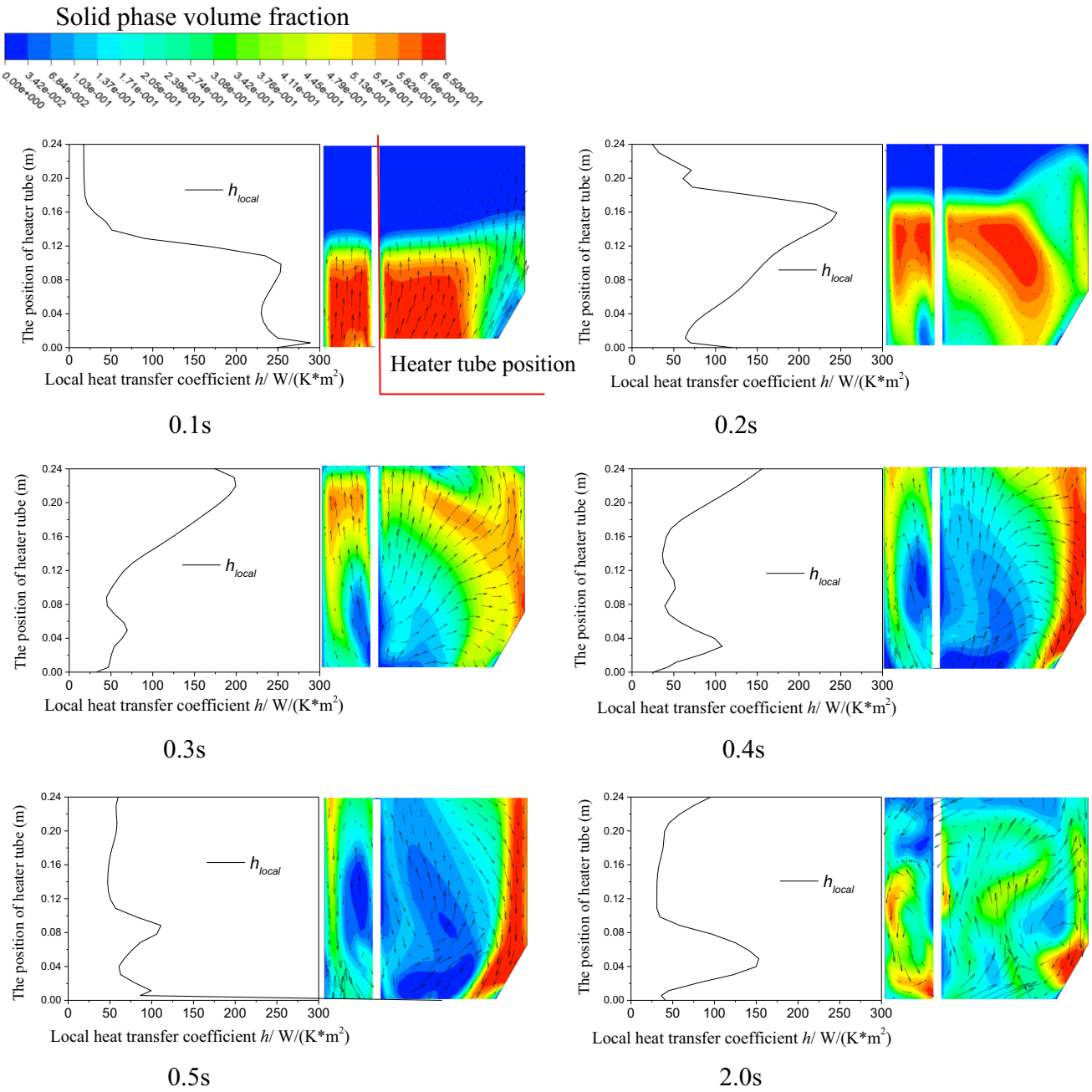

Fig. 6 Local instantaneous heat transfer coefficients (h) and solid volume fraction around heater surface at different numerical time ($U_H = 2.57$ m/s, $U_L = 0.69$ m/s, $U_F = 0.68$ m/s, $Q = 10.0$ m^3/h, $H = 20$ cm, $q = 46{,}419$ W/m^2)

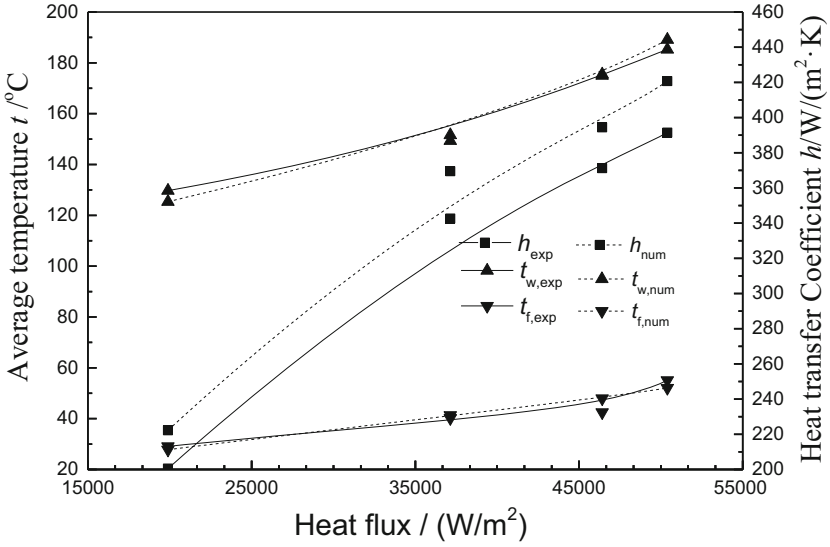

Fig. 7 Variation of steady-state surface and fluid temperature and average heat transfer coefficient against heat flux (U_H = 2.57 m/s, U_L = 0.69 m/s, U_F = 0.68 m/s, Q = 10.0 m^3/h, H = 20 cm)

the higher the concentration of solid particles is, the higher the convective heat transfer coefficient is. Therefore, the convective heat transfer coefficient of solid particles is the main component of heat transfer in the dense phase zone of the bottom of the inner circulating fluidized bed, and sometimes it can even play a dominant role, that is to say, the solid-phase particles are the main heat-carrying medium in the process of convective heat transfer.

5.3 Effect of input heat flux

In the course of numerical simulation of the experiment, a constant heat flux density was used to simulate the uniform heating of a cylindrical resistive heater. The value of the constant heat flux was the same as the actual experimental value. Figure 7 shows the variation of mean fluid temperature and heating surface temperature and convection heat transfer coefficient between fluid and heating surface at different heating heat flux density in an internal circulating fluidized bed obtained by experiment and numerical simulation. It can be seen from the figure that the heating heat flux changes from 19,849 W/m2 to 50,398 W/m2 during the process, in which the high-speed air intake is equal to 2.57 m/s, the low-speed air intake is equal to 0.69 m/s, and the cross-wind air intake is equal to 0.68 m/s, with the total inlet air flow equal to 10 m3/h, the numerical simulation predicted the average convection heat transfer coefficient from 225 W/(K . m2) to 420 W/(K . m2). The average convection heat transfer coefficient h shows the same trend by experiment and numerical simulation, and the simulated value is slightly higher than the experimental value. This is due to that it is difficult to achieve absolute thermal insulation of the outer wall surface under experimental conditions. The simulated average temperature of the heated surface increases from 127 °C to 186 °C, and the simulated average fluid temperature is from 29.1 °C to 45.0 °C. The experimental and numerical results show that the average temperature of the heating wall and the fluid are in good agreement with each other and the trend is the same.

5.4 Effect of solid mass flux across the opening orifice

Table 5 is the particle circulation volume obtained under different air intake speed conditions. From the corresponding conditions in the table, we can find that with the cross-wind airspeed U_F = 0.68 m/s, with the difference of the high and low air intake speed from 0.87 m/s increased to 1.88 m/s, and the particle circulation volume monotonically increased from 60.7 kg/m2•s to 197.16 kg/m2•s. The Bernoulli energy equation shows that the pressure difference (ΔP_0) between the beds on both sides of the internal circulating fluidized bed separator increases with the increase in the velocity difference (U_H - U_L). From the eq.1, the particle circulation volume is positively correlated with the pressure difference (ΔP_0) between the beds on both sides of the internal circulating fluidized bed separator. It can be seen from Fig. 8 that the average temperature of the heated wall by

Table 5 Solid mass flux in various operational condition(U_F = 0.68 m/s)

Operational condition	U_H = 1.74 m/s U_L = 0.69 m/s	U_H = 1.74 m/s U_L = 0.87 m/s	U_H = 2.57 m/s U_L = 0.69 m/s	U_H = 2.57 m/s U_L = 0.87 m/s
U_H - U_L(m/s)	1.05	0.87	1.88	1.70
Solid mass flux W (kg/m^2·s)	95.89	60.77	197.16	118.93
Total volume flux Q(m^3/h)	9.0	10.0	11.4	12.4

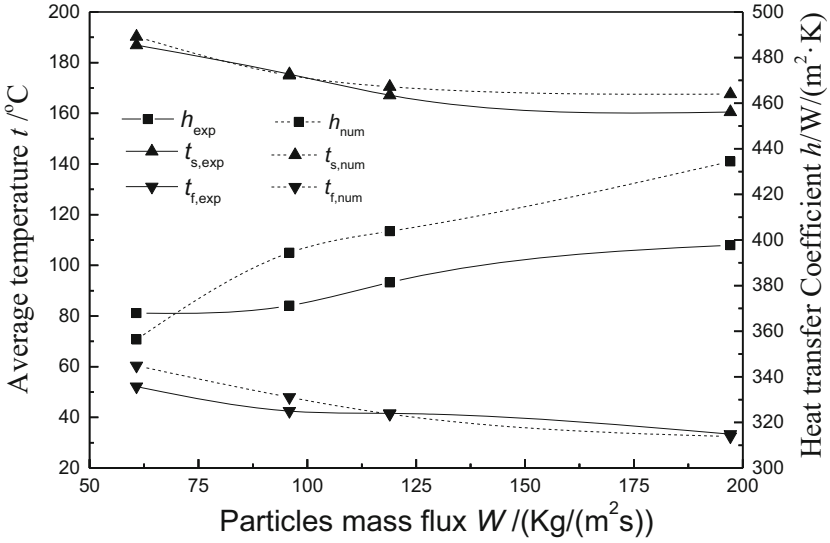

Fig. 8 Variation of the steady-state surface, fluid temperature and average heat transfer coefficient with different solid mass flux (H = 20 cm, q = 46,419 W/m^2)

experiment and numerical simulation decreases from 185 °C to 160 °C as the particle circulation at the orifice increases from 61 Kg/(m2•s) to 197 Kg/(m2•s), the average temperature of the fluid slowly decreases from 60 °C to 32 °C, and the convective heat transfer coefficient increases. This is due to the fact that as the amount of particle circulation volume at the orifice increases, the flow of particles passing over the surface of the heating tube increases, causing the fluid particles to carry more heat away from the higher temperature heating surface, this makes the average temperature of the heated wall decreasing. The average temperature of the fluid showed a decreasing trend, which was due to the fact that the increase in the amount of blowing air from the surface of the particles at a high speed, which caused the average temperature of the dense phase region to decrease. Comparing the results of experiments and simulations, it can be found that both have the same trend of change and the average temperature and convective heat transfer coefficient tend to be consistent within a reasonable range.

5.5 Effect of initial solid packing height

Figure 9 shows the change that under the different initial solid packing height, the average temperature of the heater surface of the internal circulating fluidized bed, mean fluid temperature and the convective heat transfer coefficient between the fluid and the heated surface obtained by experiments and numerical simulations. According to experimental conditions, the initial solid packing height control in numerical simulation is realized by the solid-phase marking of the fluid field in the grid model and setting the initial material void ratio. From the figure, it can be observed that with the increase of the initial solid packing height, under the same heat flux conditions (q = 46,419 W/m2), the variation trend of average convection heat transfer coefficient obtained by experiments hexp and numerical simulations hnum is the same. The average convection heat transfer coefficient between the fluid and the heated surface is shown an upward trend by experiment and numerical simulation. During the initial

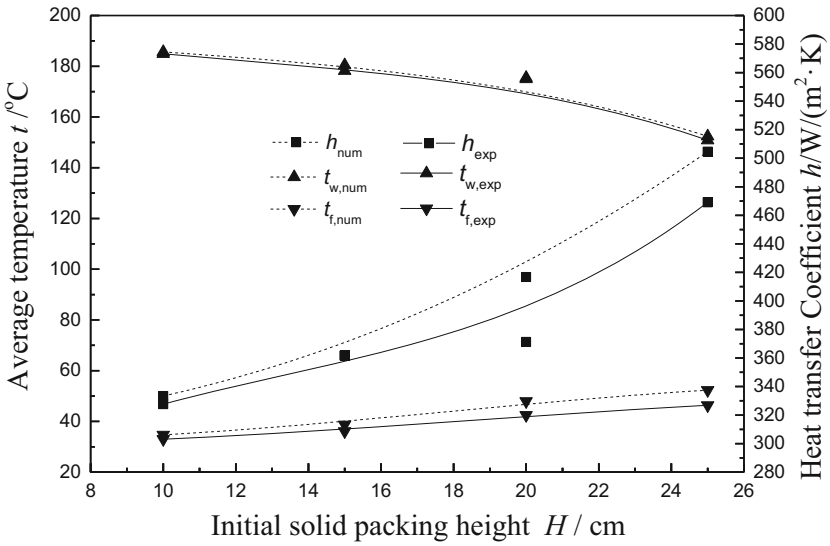

Fig. 9 Variation of steady-state surface, fluid temperature and average heat transfer coefficient with different initial solid packing height (U_H = 2.57 m/s, U_L = 0.69 m/s, U_F = 0.68 m/s, Q = 10.0 m^3/h, q = 46,419 W/m^2)

solid packing height increase from 10 cm to 25 cm, the numerical simulation predicts the average convection heat transfer coefficient hnum from 340 W/ (K . m2) increased to 505 W/(K . m2). This is due to that the increase in heat transfer efficiency the increase in heat transfer media per unit volume with the increase of initial bed material stacking height. The average temperature of the heated wall and the fluid obtained by experiments and numerical simulations agree well and with the same trend. The simulated value of the average temperature of the heated surface decreased from 185 °C to 150 °C, and the simulated value of the average fluid temperature increased from 32 °C to 50 °C.

6 Conclusions

In this chapter, the flow and heat transfer process of the inner circulating fluidized bed is numerically simulated by the Eulerian-Eulerian method. According to the actual internal circulating fluidized bed, a reasonable physical model is developed and a suitable calculation model is selected. Comparing the prediction results of numerical simulations, the main conclusions are as follows:

(1) Along the height of the bed, the velocity of the solid particles increases, to form the bottom particle acceleration zone. In the inner circulating fluidized bed, since there is a speed difference between the high-speed area and the low-speed area, lateral movement of the particles from the low-speed area to the high-speed area can be observed at the bottom of the acceleration area. In the dilute phase region, most of the particles exist as flocculants with an agglomeration state.

(2) The convective heat transfer coefficient of solid particles is the main component of heat transfer in the dense phase zone of the bottom of the inner circulating fluidized bed, and sometimes it can even play a dominant role, the solid-phase particles are the main heat-carrying medium in the process of convective heat transfer. With the increase of the initial solid packing height, the average convection heat transfer coefficient between the fluid and the heated surface is shown an upward trend obtained by experimental and numerical simulations.

(3) By comparing the average temperature of the heater surface and the average fluid temperature of the internal circulating fluidized bed under different operating conditions, including heating heat flux, inlet volume flow, and initial bed packing height, which is obtained through experimental and numerical simulations and the convective heat transfer coefficient between the fluid and the heated surface. It can be concluded that the numerical simulation of the flow and heat transfer process of the inner circulating fluidized bed by the Eulerian-Eulerian method is in good agreement with the experimental results. Field and temperature data are reasonable.

Acknowledgements The authors are grateful to the National Basic Research Development Program of China (973 Program-2011CB201506) for the financial support of this work.

References

1. Feng Y, Swenser-Smith T, Witt PJ, Doblin C, Lim S, Schwarz MP (2012) CFD modeling of gas-solid flow in an internally circulating fluidized bed. PowderTechnol 219:78–85
2. Jeon JH, Kim SD, Kim SJ, Kang Y (2008) Combustion and heat transfer characteristics in a square internally circulating fluidized bed combustor with draft tube. Fuel 87(17–18):3710–3713
3. Li P, Wang T, Liu Y, Zhang Q, Li Q, Xiong R, Guo L, Song J (2017) CFD simulation of the hydrodynamic behavior in an internally circulating fluidized bed reactor for producing polysilicon granules. Powder Technol 311:496–505
4. Simanjuntak JP, Zainal ZA (2015) Experimental study and characterization of a two-compartment cylindrical internally circulating fluidized bed gasifier. Biomass Bioenergy 77:147–154
5. Fan H, Chen B, Yang R, Guo D (2018) Experimental simulation of particle agglomeration in an internally circulating fluidized bed. Exp Thermal Fluid Sci 91:77–282
6. Luo K, Yang S, Tan J, Fan J (2015) LES-DEM investigation of dense flow in circulating fluidized beds. Procedia Engineering 102:1446–1455
7. Wei G (2017) Experimental and numerical investigation of particle flow and mixing characteristics in an internally circulating fluidized bed. Shenyang Aerospace University, Shenyang, pp 1–63
8. Meng Z, Liu M, Xie J, Wang W, Chunxi L (2018) Comparative study on the hydrodynamics and mixing characteristics of a new-type particle mixer. Powder Technol 332:90–105
9. Luo K, Fang M, Yang S, Zhang K, Fan J (2013) LES-DEM investigation of an internally circulating fluidized bed: effects of gas and solid properties. Chem Eng J 228:583–595
10. Lu Y, Zhang T, Dong X (2016) Numerical analysis of heat transfer and solid volume fraction profiles around a horizontal tube immersed in a supercritical water fluidized bed. Appl Therm Eng 93:200–213
11. Wang L, Xie X, Wei G et al (2017) Numerical simulation of hydrodynamic characteristics in a gas-solid fluidized bed. Part Sci Technol 35(2):177–182
12. Hua LN, Zhao H, Li J et al (2015) Eulerian-Eulerian simulation of irregular particles in dense gas-solid fluidized beds. Powder Technol 284(NOV):299–311
13. Gan J, Zhou Z, Yu A (2016) Particle scale study of heat transfer in packed and fluidized beds of ellipsoidal particles. Chem Eng Sci 144:201–215
14. Dong NH, Armstrong LM, Gub S, Luo KH (2013) Effect of tube shape on the hydrodynamics and tube-to-bed heat transfer in fluidized beds. Appl Therm Eng 60(1–2):472–479
15. Olsson SE, Almstedt AE (1995) Local instantaneous and time-averaged heat transfer in a pressurized fluidized bed with horizontal tubes: influence of pressure, fluidization velocity and tube-bank geometry [J]. Chem Eng Sci 50(20):3231–3245
16. Gidaspow D, He Y, Lu H (2003) Hydrodynamic modeling of binary mixture in a gas bubbling fluidized bed using the kinetic theory of granular flow [J]. Chem Eng Sci 58(7):1197–1205
17. Kuramoto M, Kunii D, Furusawa T (1986) Flow of dense fluidized particles through an opening in a circulation system. Powder Technol 47(2):141–149

18. Mostafazadeh M, Rahimzadeh M, Hamzei M (2013) Numerical analysis of the mixing process in a gas-solid fluidized bed reactor. Powder Technol 239(2):422–433
19. Ergun S (1952) Fluid flow through packed columns. Journal of Materials Science & Chemical Engineering 48(2):89–94
20. Wen CY, Yu YH (1966) Mechanics of fluidization. Chem Eng Prog Symp Ser 62(1):100–111
21. Abdelmotalib HM, Youssef MAM, Hassan AA, Youn SB, Im I-T (2015) Heat transfer process in gas-solid fluidized bed combustors: A review. Int J Heat Mass Transf 89:567–575